ACS Sustainable Chemistry & Engineering

Research Article

pubs.acs.org/journal/ascecg

One-Step Calcination of the Spent Bleaching Earth for the Efficient Removal of Heavy Metal Ions

Jie Tang,[†,‡] Bin Mu,[†] Maosong Zheng,[†] and Aiqin Wang*[,†]

[†]Center of Eco-materials and Green Chemistry, State Key Laboratory of Solid Lubrication, Lanzhou Institute of Chemical Physics, Chinese Academy of Sciences, Lanzhou 730000, People's Republic of China

[‡]University of Chinese Academy of Sciences, Beijing 100049, People's Republic of China

ABSTRACT: Attapulgite/carbon nanocomposites were fabricated via one-step calcination of the spent bleaching earth served as adsorbents for the efficient removal of heavy metal ions (Cu(II), Pb(II) and Cd(II)). The as-prepared nanocomposites were characterized by Fourier transform infrared spectroscopy, scanning electron microscopy, transmission electron microscopy, X-ray diffraction, thermogravimetric analysis and Brunauer–Emmett–Teller techniques. The process parameters affecting the adsorption behaviors such as initial pH, calcination temperature, contact time and initial concentration of heavy metal ions were systematically investigated. The results indicated that the attapulgite/carbon nanocomposites derived from the low-cost available carbon precursors exhibited high adsorption capacity within a wide pH range, and the faster equilibrium was achieved at lower concentration. In addition, the adsorbed Cu(II), Pb(II) and Cd(II) can be partially desorbed using 0.1 mol/L HCl as the desorbing agent, rendering the as-prepared adsorbent good readsorption ability, especially for the removal of Cu(II). Using the adsorption of Cd(II) as an example, it has been confirmed that the electrostatic interaction, cation exchange and surface complexation between Cd(II) and functional groups on the attapulgite/carbon nanocomposites were the dominant mechanisms according to the results of the adsorption studies and XPS analysis. Furthermore, this research develops a feasible route for the application of the spent bleaching earth in the wastewater treatment.

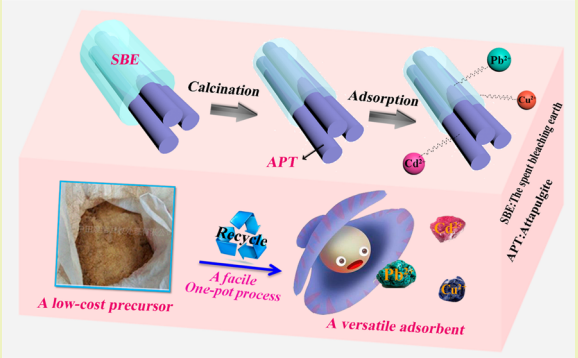

KEYWORDS: *Spent bleaching earth, Attapulgite, Carbonization, Adsorption, Heavy metal ions*

INTRODUCTION

Heavy metal ions released into the environment have increased continuously as a consequence of the rapid development of various industrial activities and technologies.[1] Heavy metals from these polluted streams can then enter into the surrounding soil, surface water and groundwater, posing a direct or indirect threat to public health because of their higher toxicities, nonbiodegradability, high capabilities in bioaccumulation in the human body, food chain and carcinogenicities to humans.[2−4] In conclusion, heavy metal pollution has become one of the serious environmental problems of worldwide concern. Heavy metals like lead, nickel, copper, zinc, cadmium and chromium are among the most common pollutants found in industrial effluents, and are nonbiodegradable and toxic even in trace amounts.[5,6] Consequently, it is urgent that some environmentally sound and practically feasible technologies or adsorbents need to be developed. At present, adsorption, as a wastewater treatment process, has been confirmed to be one of the prime techniques under investigation or exploration for remediation, restoration and sustainability of our environment from contamination,[7] owing to its enviable properties such as high efficiency, easy handling, low operational costs, availability and so on. However, it remains greatly challenging to develop a low-cost, high adsorption capacity and fast adsorption rate adsorbent.[8,9]

Clay minerals are an abundant, low-cost, nontoxic natural resource that has been found particularly useful for adsorption of heavy metals.[10] Research on the modification of clay minerals to increase their adsorbent capacity to remove heavy metals and other contaminants from drinking water is in progress. Among them, clay minerals/carbon composite, a significant extrinsic carbonaceous component arising from low cost materials, including agricultural by products, industrial wastes and biological materials, is regarded as a promising class of adsorbents for water purification and industrial wastewater treatment in recent decades.[11,12]

Palm oil is an edible, highly saturated vegetable oil that is commonly and abundantly used as a cooking ingredient, especially in the food processing industries.[13,14] Crude palm oil usually contains many impurities, coloring matters and other hazardous substances, which are bad for human health and the oil's quality. Therefore, it is indispensable to remove these components and improve the appearance and quality of the oil

Received: January 20, 2015
Revised: March 12, 2015
Published: April 17, 2015

DOI: 10.1021/acssuschemeng.5b00040
ACS Sustainable Chem. Eng. 2015, 3, 1125−1135

before eating by using activated clay minerals with a dosage of 1%−3%, and then the activated clay minerals become the spent bleaching earth (SBE) after bleaching, which contains non-hydratable phospholipids, natural pigment, fatty acid, vitamins and 10% normal grease, etc. Malaysia is the largest producer and exporter of palm oil in the international market (approximately 50% and 58%).[15] In step with the growth of the cultivation of palm oil, one of the significant problems in palm oil processing is managing of the SBE or palm shell also generated during the process. Palm oil mills in Malaysia produce about 4.3 million tonnes of shell and a considerable amount of the SBE annually as a byproduct of industrial production,[16,17] more than 50% of which are burned for the purpose of quick waste disposal and immediately discarded as garbage, or used as feed additives in formal practice.[15] Some quantity of those byproducts has not been fully utilized in a rational way. If the excess residues can be turned into useful and valuable products, our efforts can bring promise to every oil palm industry.[18] Therefore, it is crucial to promptly develop new economical technologies for SBE disposal and utilization to make the ecosystem more sustainable. To enhance the adsorption of heavy metal ions, attapulgite/carbon (APT/C) nanocomposites were prepared by a one-step calcination process using the spent bleaching earth as a cheap carbon precursor based on the synergetic effect between carbonaceous species and attapulgite (APT). The effects of initial pH, calcination temperature, contact time and initial concentration were systematically analyzed. In addition, the feasible adsorption mechanism was also proposed.

MATERIALS AND METHODS

Materials. Spent bleaching earth (SBE), which is mainly composed of APT and about 22.3% of organic matter (such as grease, natural pigment, fatty acid, etc.), was provided by The W Clay Industries Sdn Bhd (Malaysia). All the other agents were analytical grade and used without further purification, and all solutions were prepared with deionized water.

Preparation of the Attapulgite/Carbon (APT/C) Nanocomposites. 25.0 g of the SBE was calcinated under six different temperatures of 250, 300, 350, 400, 450 and 500 °C. The calcination was carried out in air atmosphere up to the final temperature with a heating rate of 12 °C/min, and kept at the final temperature for 2 h. The samples were marked as APT/C-250, APT/C-300, APT/C-350, APT/C-400, APT/C-450 and APT/C-500 corresponding to the above calcinated temperatures, respectively.

Characterization. The morphologies of the samples were observed using field emission scanning electron microscopy (FESEM, JSM-6701F, JEOL, Tokyo, Japan) at an acceleration voltage of 10.0 kV and a working distance of 10 mm at high vacuum mode after coating the sample with gold film. High resolution transmission electron microscopy (HRTEM, JEM-2010, JEOL, Tokyo, Japan) images were obtained at an acceleration voltage of 200 kV, and the sample was ultrasonically dispersed in anhydrous ethanol and dropped onto a grid before observation. Fourier transform infrared (FTIR) spectra of the samples were recorded (Thermo Nicolet NEXUS TM, USA) in the range of 4000−400 cm^{-1} using KBr pellets. The weight percent of carbonaceous species was determined by thermogravimetric analysis (TGA, STA 6000, PerkinElmer, USA) at a heating rate of 10 °C min^{-1} from 30 to 800 °C in an oxygen atmosphere. Power X-ray diffraction (XRD, Pana XPERT PRO, The Netherlands) patterns were performed using an X-ray diffractometer with a Cu Kα (1.540 598 Å) radiation at a scan rate of 0.05° s^{-1}, running at 40 kV and 30 mA. The ζ-potentials of suspensions were conducted using a ζ-potential instrument (Malvern Zeta voltmeter (ZEN3600), Britain). UV−vis spectra were determined using a UV−vis spectrophotometer (SPECORD 200, Analytik Jera AG). The specific surface area was determined by the Brunauer−Emmett−Teller (BET) method and the pore volume was estimated by the Barrett−Joyner−Halenda (BJH) method at 77 K (ASAP 2020 M, Micromeritics Instrument Corporation, USA). The samples were dried and outgassed at 105 °C for 4 h before N_2 adsorption. X-ray photoelectron spectroscopy (XPS) analysis was obtained using a VG ESCALAB 250 Xi spectrometer equipped with a Monochromated Al Kα X-ray radiation source and a hemispherical electron analyzer. The spectra were recorded in the constant pass energy mode with a value of 100 eV, and all binding energies were calibrated using the C 1s peak at 284.6 eV as the reference.

Adsorption Experiment. The stock Cu(II), Pb(II) and Cd(II) solution with a concentration of 1000 mg L^{-1} was prepared by dissolving an appropriate amount of $Cu(CH_3COO)_2$, $Pb(CH_3COO)_2$ or $Cd(CH_3COO)_2$ in distilled water. The different concentration of Cu(II), Pb(II) and Cd(II) for adsorption study were all prepared by dilution of the stock solution.

All the adsorption experiments were performed with 25 mg of adsorbent and 25 mL of the Cu(II), Pb(II) or Cd(II) solution. The mixtures were shaken with a constant speed (160 rpm) and constant temperature (30 °C) in a thermostatic orbital shaker (THZ-98A) for a given time, and then the supernatant solution was separated from the adsorbent by centrifugation. The concentrations of Cu(II), Pb(II) or Cd(II) solution before and after adsorption were measured spectrophotometrically using 2,9-dimethyl-1,10-phenanthroline, 1,10-phenanthroline monohydrate and xylenol orange as the complexing agent by monitoring the absorbance changes at the wavelength corresponding to maximum absorbance of 456, 533 and 576 nm, respectively.[19−21] The adsorption capacity of the adsorbent for Cu(II), Pb(II) or Cd(II) was calculated according to eq 1:

$$Q_e = \frac{(C_0 - C_e) \times V}{m} \quad (1)$$

where Q_e is the adsorption capacity of Cu(II), Pb(II) or Cd(II) onto the adsorbent (mg/g), C_0 and C_e are the initial and equilibrium concentrations of Cu(II), Pb(II) or Cd(II) (mg/L), m is the mass of adsorbent used (mg) and V is the volume of Cu(II), Pb(II) or Cd(II) solution used (mL).

The effects of pH on Cu(II), Pb(II) or Cd(II) adsorption were studied with the initial concentration of 200 mg/L Cu(II), Pb(II) or Cd(II) and different pH values (1.0−6.0) until adsorption equilibrium. The pH values were adjusted with 0.1 mol/L HCl or NaOH solutions.

Desorption and Regeneration Studies. The desorption of a Cu(II)-, Pb(II)- or Cd(II)-loaded nanocomposite was done using 0.1 mol/L HCl solution as the desorbing agent. 25 mg of heavy metal loaded adsorbent was contacted separately with 25 mL 0.1 mol/L HCl solution and placed in a thermostatic shaker and shaken for 240 min at 160 rpm. At the end of the experiment, the supernatant was discarded by centrifugation and the solid was washed with distilled water for three times and then employed for another adsorption. The consecutive adsorption−desorption process was performed for five times, and the adsorption capacity of the adsorbent regenerated for different times was obtained.

RESULTS AND DISCUSSION

To deepen the reuse of SBE through an environmentally friendly way and to realize the sustainable development and cyclic utilization of APT's industrial chain, a promising option was converting them into a prospective carbon precursor for the preparation of novel adsorbent. In the present study, the APT/C nanocomposites were prepared by one-step calcination process, and then those adsorbents were applied for the removal of Cu(II), Pb(II) and Cd(II) from an aqueous solution to evaluate their feasibilities as a novel adsorbent in environmental remediation. The continuous column adsorption studies suggested that this adsorbent has promising potential for the adsorption of the heavy metal ions from wastewater, as illustrated in Scheme 1.

DOI: 10.1021/acssuschemeng.5b00040
ACS Sustainable Chem. Eng. 2015, 3, 1125−1135

Scheme 1. Schematic Illustrating the Synthetic Route of the APT/C Nanocomposites

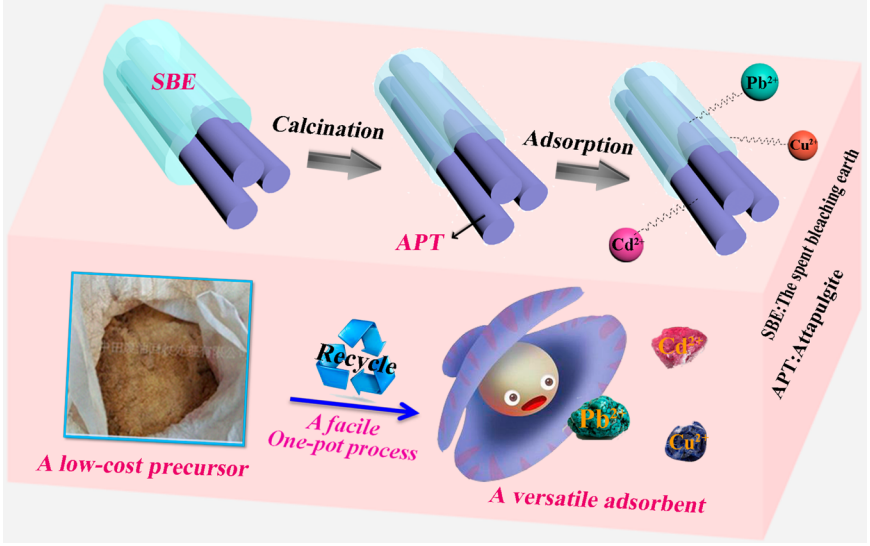

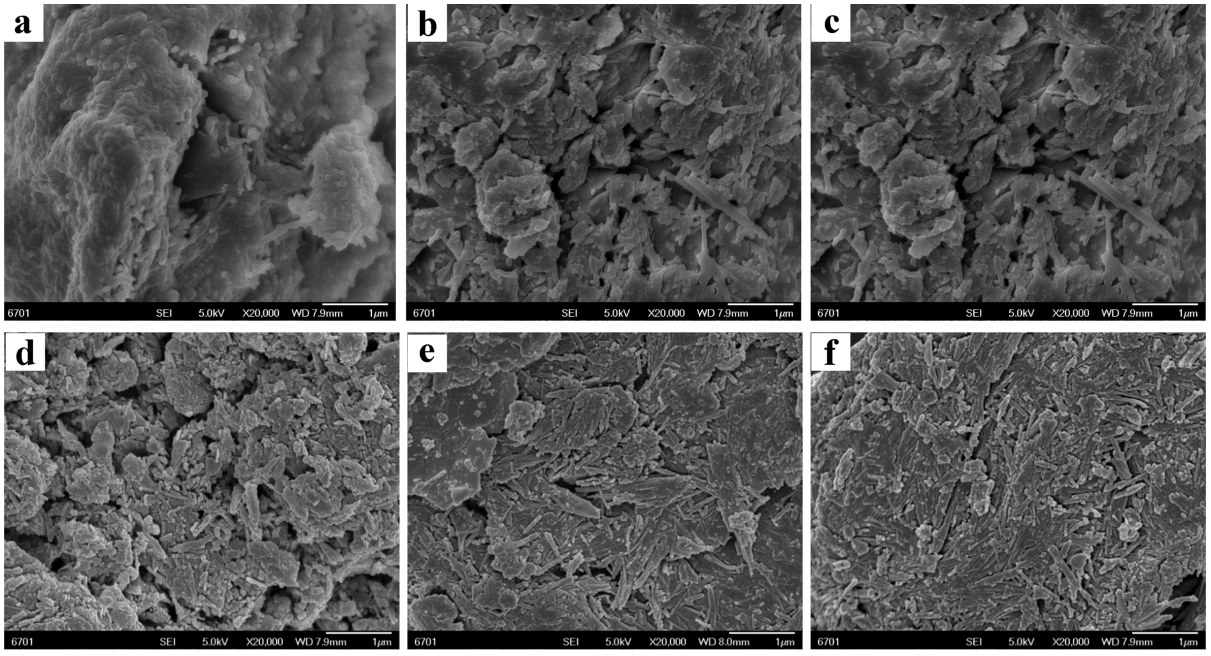

Figure 1. SEM images of (a) APT/C-250, (b) APT/C-300, (c) APT/C-350, (d) APT/C-400, (e) APT/C-450 and (f) APT/C-500.

Characterization of the Adsorbents. Typical SEM of APT/C nanocomposites clearly reveal the rod-like morphology (Figure 1), which is attributed to the typical structure of APT. Due to the existence of van der Waals force and hydrogen bonds, the single crystals of APT are inclined to crystal bundles and aggregates.[22] The nanorod-like APT gradually increases with the elevated calcination temperature, implying that the increase of calcination temperature is favorable to improve the aggregate phenomenon of crystal bundles and aggregates. This phenomenon is caused by the decomposition of the carbonates. As shown in the TEM images of the representative product of APT/C-300 (Figure 2), it can be found that APT is rod-like in shape with a length 0.4−1.0 μm and a diameter of 10−40 nm. Furthermore, it is also obvious that the carbon species are formed during calcining process. The combination of carbon species and functional groups of APT is expected to enhance the adsorption of metal ions.

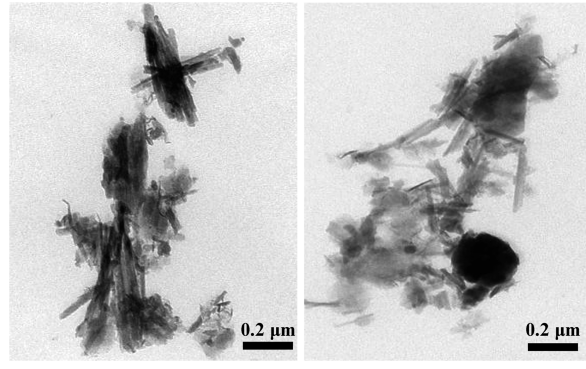

Figure 2. TEM images of APT/C-300.

FTIR spectroscopy is further employed to study the functional groups on the APT before and after being calcinated.

DOI: 10.1021/acssuschemeng.5b00040
ACS Sustainable Chem. Eng. 2015, 3, 1125−1135

The FTIR spectra of SBE and APT/C nanocomposites calcinated at different calcination temperatures (200, 250, 300, 350, 400, 450 and 500 °C) are compared in Figure 3. SBE

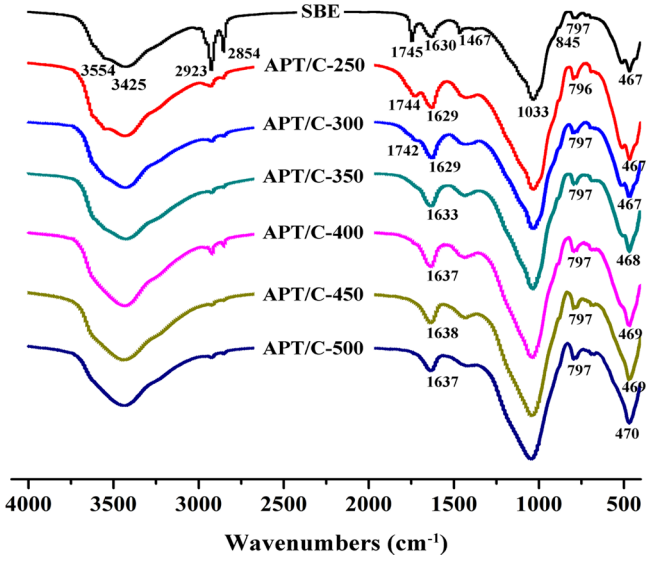

Figure 3. FTIR spectra of SBE and APT/C nanocomposites.

shows the absorption bands at 2923 and 2854 cm^{-1}, which is related to the C—H stretching vibration of $-CH_3$, $-CH_2-$ and C−H.[23] After calcination, this absorption band disappears, which is direct evidence that the residual organic matters have been transformed into carbon species during the heat treatment process. Furthermore, for SBE, the peaks at 3554, 3425 and 1630 cm^{-1} are attributed to the −OH stretching and bending vibrations of the adsorbed water, respectively. After calcination, the intensities of these peaks decrease obviously or even disappear because of the removal of the adsorbed water and the hydroxyl groups.[24] In addition, the presence of the carboxyl groups is testified by the absorption band of the C═O stretching vibration at 1745 cm^{-1}. The relative intensity of the C═O stretching vibration at 1745 cm^{-1} to the bending vibrations of the adsorbed water at 1630 cm^{-1} greatly decreases after being calcinated at 250 and 300 °C, even the characteristic absorption band at 1745 cm^{-1} almost disappears while the calcination temperature is above 300 °C, meaning that the adsorption capacity of APT/C nanocomposites may be affected by this change. For SBE and APT/C nanocomposites, the peaks at 1467 and 845 cm^{-1} corresponding to the asymmetrical stretching vibration and bending vibration of carbonate are observed, respectively, which are indicative of the existence of a small quantity of carbonates in the samples. The intensities of these peaks are weakened after being calcinated, implying that the decomposition of carbonates. The characteristic of the absorption band of the C—C band at 467 cm^{-1} might be overlapped with the bending vibration of Si—O at 468 cm^{-1}.

To confirm further the existence of carbonaceous materials, three APT/C nanocomposites, APT/C-250, APT/C-300 and APT/C-450, were selected for mass loss analysis. The thermogravimetric analysis (TGA) curves are shown in Figure 4. In the crystal structure of APT, there are four different states of water, which can be selectively removed by controlling thermal treatment temperature.[25,26] The TGA curves revealed the dehydration/dehydroxylation of APT and the decomposition of organic matters on the surface of APT.[27] For APT,

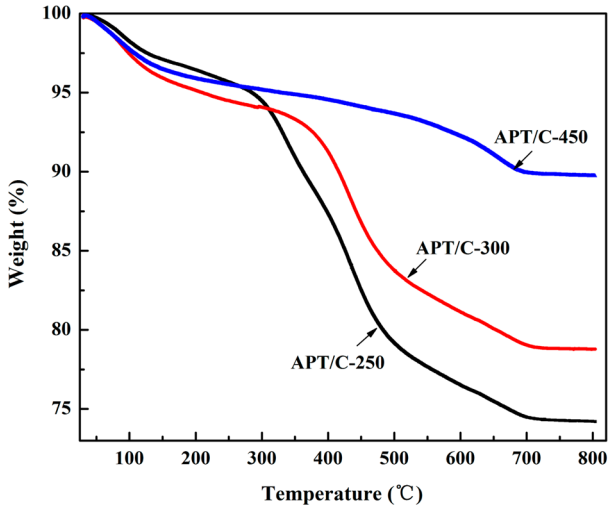

Figure 4. TGA curves of APT/C-250, APT/C-300 and APT/C-450.

the first step of the mass loss that occurs below 230 °C is attributed to the release of the adsorbed water physically bonded to APT on the external surface or in the structural channels and zeolitic water. The second dehydration step that occurred at approximately 230−400 °C is also observed, which can be assigned to removal of a majority of the coordinated water. The residual coordinated water molecules and hydroxyl structural water were linked to the third and fourth step mass losses occurs at 400−600 and over 600 °C, respectively.[28] For APT/C nanocomposites, the main mass loss below 200 °C is similar to that of APT, but that between 200 and 600 °C can be assigned to the combustion of organic matter under oxygen atmosphere.[29] In the temperature range, the mass loss about 17.25%, 11.36% and 2.23% for APT/C-250, APT/C-300 and APT/C-450, respectively. For APT/C-300 and APT/C-450, the mass losses at this stage were obviously lower than that for APT/C-250, indicating the more content of organic matter in APT/C-250. Along with the temperature increases, the mass loss of APT/C nanocomposites is obviously reduced, indicating that the carbon content of nanocomposites gradually decreased.

X-ray diffraction analysis is an important method for identifying mineral species. Three samples, SBE, APT/C-300 and APT/C-450, were characterized using X-ray diffraction (XRD), as shown in Figure 5a. The XRD pattern of SBE exhibits main diffraction peaks corresponding to the characteristics of the APT, which is consistent with the results reported previously. The characteristic diffraction peak of APT was found at about 2θ = 8.4° (110 plane, d = 1.05 nm), 13.7° (200 plane, d = 0.64 nm), 16.4° (130 plane, d = 0.54 nm), 19.8° (040 plane, d = 0.45 nm), 21.5° (310 plane, d = 0.41 nm), 27.5° (400 plane, d = 0.32 nm), 34.7° (102 plane, d = 0.26 nm) and 42.5° (600 plane, d = 0.21 nm).[30,31] In addition, the diffraction peaks at 2θ = 20.9°, 26.6°, 36.6°, 50.2°, 60.1° and 68.4° were characteristic peaks of quartz, and the diffraction peaks at 2θ = 30.9° and 39.6° were due to the dolomites, indicating that the APT contains quartz and small amounts of dolomites.[32−34] As shown in Figure 5a, the APT/C nanocomposites show the similar characteristic diffraction peaks to those of the pristine SBE, indicating the preservation of the structural features of APT after the calcinations process. Comparing the XRD patterns of SBE and APT/C-300, there is no obvious difference among the scattering peaks from the two samples, which demonstrates that the structure and crystallinity of APT were

DOI: 10.1021/acssuschemeng.5b00040
ACS Sustainable Chem. Eng. 2015, 3, 1125−1135

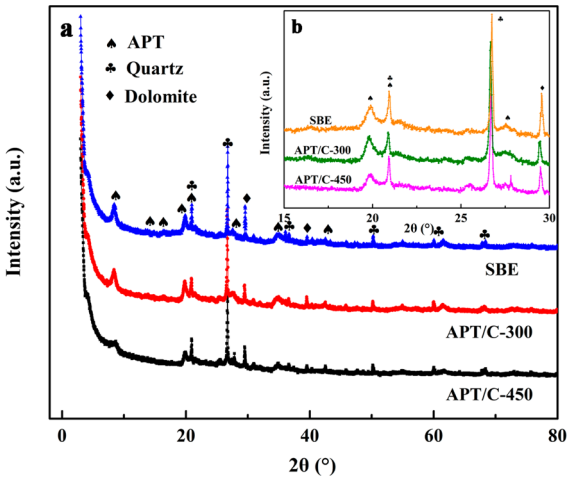

Figure 5. XRD patterns of (a) SBE, APT/C-300 and APT/C-450 and (b) partial enlarged view of SBE, APT/C-300 and APT/C-450.

maintained perfectly in APT/C-300. For APT/C-450, the characteristic peaks of APT change slightly and the intensity decrease evidently compared with other two samples, indicating that a higher calcination temperature could decrease the aggregation of crystal bundles or aggregates and destroy the crystal structure of APT. Therefore, it is worth noting that calcination, especially at high temperatures, has a significant impact on the crystal structure of APT, which could induce a change in its adsorption capacity for heavy metal ions.[35] Overall, SBE calcined at different temperatures will show different adsorption capacities for heavy metal ions.

Figure 5b only represents the regions of 2θ from 15° to 30° in order to identify the difference clearly. It can be observed that the broad peak centered at 20°, corresponding to the amorphous carbon, might be overlapped with the diffraction peaks of APT. For the XRD patterns of the APT/C-300 and APT/C-450, the intensity of the broad peak centered at 20° weakened compared with that of the raw SBE, which might be related to the loss of the carbon species with the increase in the calcination temperature. Based on the above analysis, it can be safely concluded APT/C nanocomposites are successfully prepared.

The surface electrical characteristic of adsorbent was investigated by the ζ-potential before studying adsorption performance to predict adsorption capacity and clarify mechanism. Figure 6a shows the ζ-potential of APT/C nanocomposites obtained at different calcinations temperature. It can be seen that the zeta potential values for all the APT/C nanocomposites are negative, indicating their negatively charged surface. By comparison, the more negative potential value for APT/C-250 is observed compared with other APT/C nanocomposites, which might be attributed to the incomplete carbonization of the residual organic matters at the low calcination temperature exhibiting the digital photograph of the samples in ethanol (inset of Figure 6a). Therefore, APT/C-300 is selected to study the changes of the ζ-potential at different pH values (2.0−8.0) to understand well the adsorption mechanism, as shown in Figure 6b. APT/C-300 maintained negative ζ-potentials in the whole pH range, and even became increasingly negative as the pH values of the suspension increased, meaning that some of the function groups, for example carboxylic groups, are located at the surface of the APT/C-300 that play an important role in retaining the cationic contaminants. Thus, it can be seen that electrostatic interaction could be one of the major mechanisms controlling the adsorption of heavy metal ions on APT/C nanocomposites. In summary, the introduction of carbon species can provide an advantage for the removal of heavy metal ions under wider environmental pH conditions.

Specific surface area and pore structure parameters of adsorbents have a crucial role in the evaluation of the adsorption capacity. A summary of specific surface area and pore structure parameters of SBE and APT/C nanocomposites is listed in Table 1. For SBE, the pores might be filled with the residual organic matters, so the pore structure parameters such as specific surface area and pore diameter are very small. By contrast, it can be seen that the specific surface area of APT/C nanocomposites increases obviously in the range of 250−450 °C, and then decreases distinctly with further increases in temperature. Moreover, the variation trend of the pore volume of APT/C nanocomposites at different calcination temperatures is similar to that of the specific surface area. The above results may be related to the removal of zeolite water, coordinated water or hydroxyl structural water, the decom-

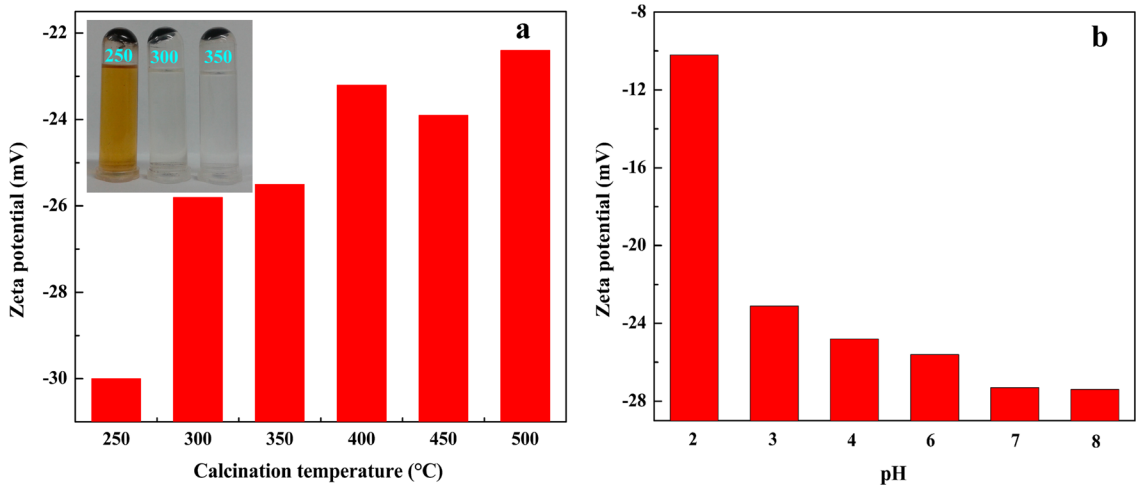

Figure 6. ζ-Potential of (a) APT/C nanocomposites at different calcination temperatures (inset of the digital photograph of APT/C-250, APT/C-300 and APT/C-350 in ethanol), and (b) APT/C-300 in the pH range of 2.0−8.0.

DOI: 10.1021/acssuschemeng.5b00040
ACS Sustainable Chem. Eng. 2015, 3, 1125−1135

Table 1. N_2 Adsorption/Desorption Analyses of APT/C Nanocomposites

sample	S_{BET} (m^2/g)[a]	S_{mic} (m^2/g)[b]	S_{ext} (m^2/g)[c]	V_{tot} (cm^3/g)[d]	D_{pore} (nm)[e]
SBE	2.34		3.49	0.002	3.85
APT/C-250	18.70		21.07	0.064	13.62
APT/C-300	41.32		50.79	0.127	12.29
APT/C-350	51.03	3.43	64.41	0.147	11.53
APT/C-400	73.29	11.59	83.77	0.173	9.45
APT/C-450	80.26	15.95	87.89	0.182	9.09
APT/C-500	68.86	11.34	81.47	0.179	10.41

[a]BET (Brunauer–Emmett–Teller) surface area. [b]Micropore surface area, derived from *t*-plot method. [c]External surface area, calculated using *t*-plot method. [d]Total pore volume, measured at P/P_0 = 0.974. [e]Average pore diameter, calculated by D_{pore} = 4 V/A according to BET.

position of the carbonates and the structure change of APT at different calcination temperatures. The removal of water below 450 °C contributes to the increase in specific surface area of the sample to some extent, and then to the improvement of the adsorption properties. When the temperature rises to 500 °C, the remaining coordinated water and a small amount of hydroxyl structural water are removed, which result in folding of the APT pores. Such a reduction also can be attributed to the decomposition of the loaded carbon species that covered, or partially filled the channel of APT during calcination process. Those two mutual effects result in a lower adsorption capacity for heavy metal ions. The variation of adsorption capacity of the heat-treated APT toward cadmium ion is consistent with that of the specific surface area of heat-treated APT with the elevated temperature.[36] The above results reveal that the calcination temperature, which resulted in a significant change in the pore structure, really is the dominant factor affecting the adsorption capacity of APT/C nanocomposites for heavy metal ions.

Adsorption Property. To optimize the adsorption systems for the removal of Cu(II), Pb(II) and Cd(II) from aqueous solution, it was important to investigate the equilibrium properties of the adsorption process. Calcination temperature is a crucial factor of determining the adsorption capacity of APT/C nanocomposites. All of the samples are evaluated and the results displayed in Figure 7. It can be seen that the adsorption capacity of the APT/C nanocomposite to Cu(II), Pb(II) and Cd(II) first gradually increases with increases in calcination temperature in the range of 250–300 °C, and reaches the maximum at 300 °C, and then a significant decrease is apparent from 300 to 350 °C. But in the temperature range from 350 to 450 °C, there is a slight increase for the adsorption capacity for Pb(II), and there is not a difference for the adsorption capacities of Cd(II) and Cu(II). The adsorption capacity of an adsorbent is related to its own surface functional groups and pore structure parameters such as specific surface area and pore diameter, and the combination of these leads to the final adsorption results. When SBE was calcinated at the lower calcination temperatures, keeping the structure of APT, the zeolite water and a part of the coordinated water are removed, which lead to the release of micropores to provide the access for heavy metal ion bonding. The FTIR spectra and ζ-potential are indicative of existing abundant functional groups such as hydroxyl groups, carboxyl groups, etc., which make a big difference in enhancing the adsorption capacity of heavy metal ions. Conversely, the functional groups existing on the surface of APT disappear gradually with increasing temperatures, as indicated from FTIR analysis. In addition, a higher calcination temperature can induce a decrease in the size of this pore due to folding and collapse of nanotunnels of APT, which results in a decrease in the adsorption capacity of APT/C nanocomposites at high calcination temperatures. The conclusion that APT/C nanocomposites prefer heavy metal ions adsorption in the sequence Pb(II) > Cd(II) > Cu(II) can be drawn from Figure 7. This may be explained by the different hydration energies of each ion, which can reflect the capability for the ion to interact with the functional groups on the APT/C nanocomposite surface.[37] Moreover, a list of representative studies is presented in Table 2. The APT/C-300 has a much higher adsorption performance compared with the adsorbents based on agricultural or industrial waste material. Therefore, APT/C nanocomposites prepared via one-step calcination can be used directly as an efficient and eco-friendly adsorbent for

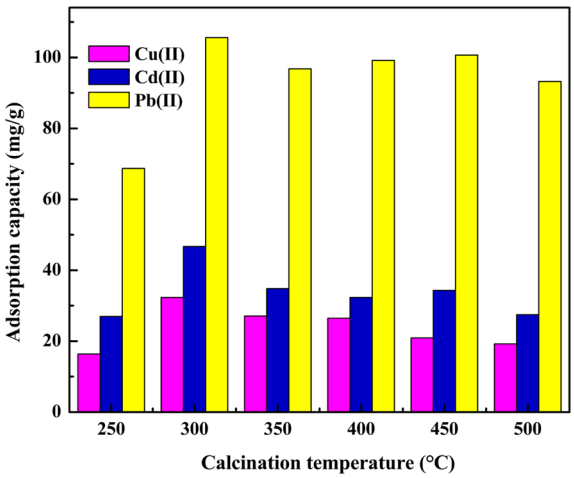

Figure 7. Effect of calcination temperature on adsorption capacity of Cu(II), Pb(II) and Cd(II).

Table 2. Comparsion of Maximum Adsorption Capacity (Q) for Cu(II), Pb(II) and Cd(II) with Various Biomass-based Biochar Adsorbents

			Q(mg/g)			
adsorbents	pH	C_0[a] (mg L^{-1})	Cu(II)	Pb(II)	Cd(II)	ref
fresh swine manure	5.0	200	9.32			38
oak wood	5.0	100		9.49	2.80	39
sugarcane bagasse	6.0	200	3.65	21.28		40
coconut tree sawdust	6.0	200	3.89	25.00		40
cotton fiber	5.0	200	6.12	21.62	8.22	41
coconut dregs	7.0	100	2.76	9.74		42
mangosteen peel	7.0	200	21.74			43
magnetic oak bark	5.0	100		30.20		44
oak bark char	5.0	100			5.40	45
jujube complex bead	6.0	200	3.64	2.93		46
spent bleaching earth	6.0	200	32.32	105.61	46.72	this study

[a]C_0: initial concentration.

DOI: 10.1021/acssuschemeng.5b00040
ACS Sustainable Chem. Eng. 2015, 3, 1125–1135

the removal and recovery of heavy metal ions from effluent due to the advantages over traditional adsorbents, such as preparation method, property and saving energy, etc.

It is well-known that the adsorption behaviors of metal ions by an adsorbent are highly dependent on the initial pH of solution. Indeed, pH affects the transition metal speciation and changes the charge distribution on the adsorbent. Figure 8 shows the effects of solution pH on the adsorption capacity of APT/C nanocomposites for Cu(II), Pb(II) and Cd(II). Overall, it can be found that the adsorption capacities of the APT/C composites for targeted heavy metal ions have a similar variation trend within the pH range studied. The adsorption capacity shows a rapid increase at elevated initial pH values (1.0−4.0), and after that, when the pH increases up to 6.0, the increasing tendency begins to level off. Based on ζ-potential analysis, APT/C-300 is an ionic nanocomposite matrix at various pH values and its surface charge is essentially affected by changing the pH values. At the lower pH values (highly acidic), the carboxyl groups in nanocomposites are converted to carboxylic acid groups, which can weaken the electrostatic interaction of APT/C-300 with heavy metal ions and reduce the number of surface active sites available for metal ions uptake, by which the adsorption capacities for Cu(II), Pb(II) and Cd(II) decrease appreciably. In the meantime, a large amount of hydrogen ions in the solution can compete with heavy metal ions to make the ion-exchange reaction. On the contrary, at the higher pH values, more ionized carboxylic groups will be available, so the negative surface active sites would be increased, thereby increasing electrostatic interaction between positively charged heavy metal ions and the surface of the adsorbent and making the nanocomposites show higher affinity to the heavy metal ions.[44,47] With the pH increased (initial pH > 6), the adsorption site are expected to increase because more carboxyl groups can lose their hydrogen ions, resulting in more carboxylate groups within the nanocomposite. But in this range, Cu(II), Pb(II) and Cd(II) can precipitate as insoluble hydroxides.[48] This adsorption behavior of the APT/C nanocomposites at various pH values suggests that it can be potentially applied in a wide pH range. In this study, the pH values of the freshly prepared Cu(II), Pb(II) and Cd(II) solutions were determined to be 5.64, 5.56 and 6.15. Thus, the original pH values of the Cu(II), Pb(II) and Cd(II) solutions do not need to be adjusted for the following adsorption experiments.

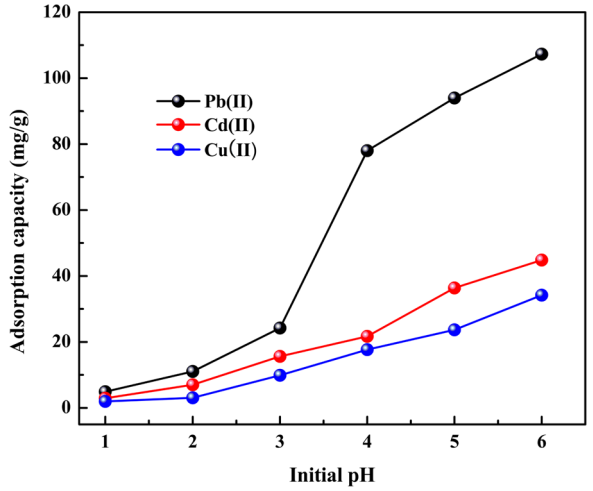

Figure 8. Effect of initial pH on the adsorption of APT/C-300 toward Cu(II), Pb(II) and Cd(II).

To understand better the adsorption process, another parameter seems also indispensable: the contact time until the adsorption system reaches its equilibrium.[49] The effect of contact time on the adsorption capacity of APT/C-300 is illustrated in Figure 9. The results clearly indicate that the adsorption of Cu(II), Pb(II) and Cd(II) onto the APT/C-300 is rapid and most of the heavy metal ions can be adsorbed approximately within 4 h. Based on Figure 9, a very fast adsorption rate is obtained in the first 2 h, which may relate to the high availability of the adsorption sites. When the adsorption sites are occupied by the metal ions, metal ions may form aggregates around the active sites, which of course creates a case of saturation of the adsorbent surface by the metal ions. That is to say, the adsorption capacity hardly increased with prolonged time, and then remained constant until the adsorption equilibrium. Consequently, the targeted ions can be accessible to the active adsorption sites and are trapped quickly by APT/C-300.

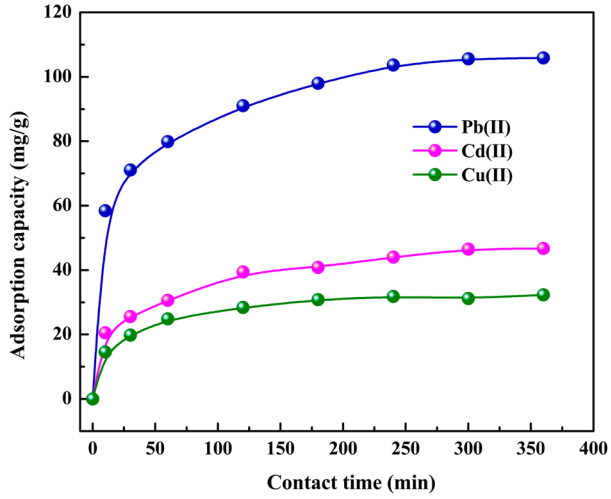

Figure 9. Effect of contact time on adsorption capacity of APT/C-300 for Cu(II), Pb(II) and Cd(II).

Except for high adsorption capacity and fast adsorption rate, initial concentration is also a decisive parameter for exploring the interaction mechanism of the adsorbent with the adsorbate. Initial concentrations of Cu(II), Pb(II) and Cd(II) from 5 to 300 mg/L are varied to study the effect of concentration on the adsorption process (Figure 10). As can be seen, the adsorption amount of targeted heavy metal ions increased as the initial concentration increased (5−200 mg L^{-1}), and then the adsorption capacities showed no further visible changes (200−300 mg L^{-1}), and faster equilibrium was achieved at lower concentrations. This was attributed to availability of sufficient vacant active sites at lower concentration which had limited adsorbates molecules to occupy on adsorbent. The superfluous unsaturated vacant sites present in the adsorption process at low concentrations transformed into lower adsorption uptake of pollutant from solution. A similar observed scenario has been reported.[50] On the other hand, a higher initial concentration will generate a stronger driving force resulting from the concentration gradient, which can increase the diffusion tendency of heavy metal ions into the adsorbent. When the initial concentration reached about 200

DOI: 10.1021/acssuschemeng.5b00040
ACS Sustainable Chem. Eng. 2015, 3, 1125−1135

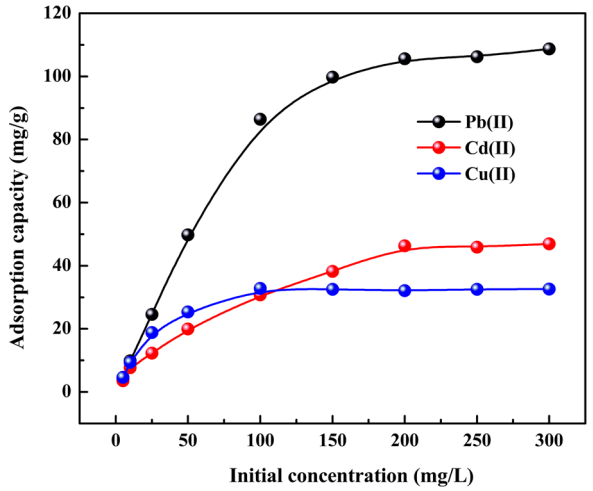

Figure 10. Effect of initial concentration on adsorption capacity of APT/C-300 for Cu(II), Pb(II) and Cd(II).

mg L^{-1}, the active adsorption sites of the adsorbent were almost occupied by Cu(II), Pb(II) and Cd(II) completely, and thus the adsorption capacity reached the maximum and almost kept constant.

Desorption and Reusability. For the adsorbent to be practically useful, the success of the adsorbent, for environmental and economic reasons, depends on the possibility of desorbing the target contaminant and reusing the adsorbent. HCl is an important desorbing agent for recovering the adsorbent used for heavy metals removal.[51,52] In this study, heavy metal ions adsorbed APT/C-300 nanocomposites were treated with 0.1 mol/L HCl solution as the desorbing agent to investigate the regeneration ability of developing a carbonaceous adsorbent. When the spent adsorbent was recovered, the reusability was evaluated, as shown in Figure 11. The

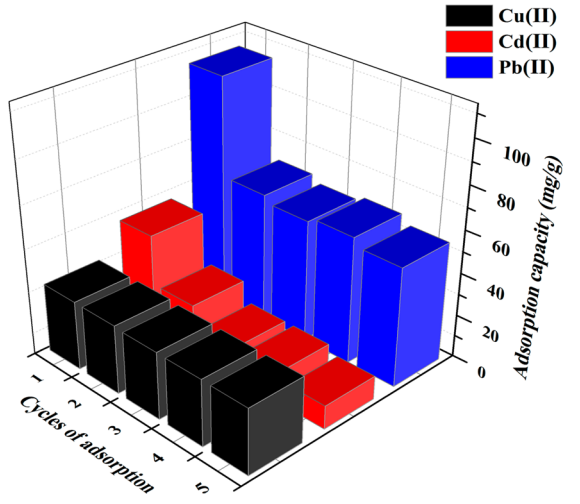

Figure 11. Reusability of the as-prepared APT/C-300 for Cu(II), Pb(II) and Cd(II) adsorption.

adsorption−desorption performance after the five-time consecutive process is excellent for Cu(II), though the adsorption capacity for Pb(II) and Cd(II) is observed to decrease evidently with increasing the cycles of adsorption, which might be attributed to their different hydration energy.[37] This may indicate that the interaction between Pb(II) or Cd(II) and the functional groups on the surface of nanocomposite is stronger than that of Cu(II). As discussed above, the as-prepared adsorbent has the potential to be developed into an efficient adsorbent for the simultaneous removal and recovery of heavy metal ions, especially for Cu(II) removal.

Adsorption Mechanism. XPS analysis was employed to identify the coordination types between heavy metal ions and these functional groups. The XPS analysis, exceptionally Cd(II), was only performed to study the changes of binding energy of C 1s and O 1s in APT/C-300 before and after adsorption (Figure 12). The results from survey scanning spectra suggested that the APT/C-300 was composed of Mg, Al, Si, C, O and Fe, which are the basic elements in attapulgite,[53] except carbon. After adsorption, another new peak was originated from the binding energy spectrum of Cd 3d, indicating Cd(II) were adsorbed on the nanocomposite (Figure 12a).

The spectra of C 1s for the APT/C-300 before and after Cd(II) adsorption are presented in Figure 12b,c. The C 1s spectra of these two samples can be curve-fitted into six individual peak components, which come from the different groups and overlap each other. As seen in Figure 12b, C 1s spectra of the APT/C-300 before Cd(II) adsorption comprise six peaks with differentiated binding energy values by deconvolution. The peaks can be assigned to the carbon atoms in the forms of >C═O (carbonyl, 284.5 eV), C—C (284.9 eV), −C—O (phenolic, alcohol or ether, 286.2 eV), CH_x (287.6 eV), −COOH (288.4 eV) and −COOR (289.2 eV), respectively,[54−56] confirmed by FTIR analysis. After the adsorption of Cd(II) (Figure 12c), their C 1s spectra show that the binding energies of the peaks have a certain degree of shift compared with that of APT/C-300 before Cd(II) adsorption. Especially, the binding energy of 284.5 eV, characteristic for >C═O, has a greater shift degree.

Similarly, three characteristic peaks were separated for the O 1s spectrum in the APT/C-300 before and after Cd(II) adsorption, as shown in Figure 12d,e. It is clear that the peaks at binding energies of 531.1, 532.0 and 532.6 eV for the APT/C-300 before adsorption can be assigned to the oxygen atom in the forms of −COOH/>C═O, C—O—(C,H) and −COOR/$-RCO_3$, respectively.[57−59] Compared to original APT/C-300, the binding energy of O 1s on the surface of nanocomposites after adsorption increased slightly, indicating that the O atom was an electron donor during Cd(II) sorption. This observation revealed that the Cd(II) adsorption on surface of the APT/C-300 was likely performed through the formation of hydroxyl−Cd, carboxyl−Cd or ketone−Cd complex species.[60]

This hypothesis can be further consolidated by the XPS spectra of Cd 3d for the APT/C-300 after adsorption (Figure 12f), The Cd $3d_{5/2}$ peak could be divided into three separate peaks at 405.3, 405.6 and 406.1 eV. The peaks at 405.3 and 405.6 eV correspond to $CdCO_3$ and $Cd(OH)_2$, respectively.[60,61] The peak at 406.1 eV is similar to the results for Cd(II) adsorption on sepiolite.[61]

The XPS analysis and Cd(II) adsorption studies indicated that the adsorption mechanism was mainly attributed to chemical interaction (electrostatic attraction, ion exchange and surface complexation) between Cd(II) and the surface functional groups of the adsorbents. The protons in the carboxylic and phenolic groups of the carbons could exchange with the cationic Cd(II) species. The deprotonated carboxylic and phenolic groups could enhance Cd(II) adsorption by electrostatic interaction. The O atoms in deprotonated

DOI: 10.1021/acssuschemeng.5b00040
ACS Sustainable Chem. Eng. 2015, 3, 1125−1135

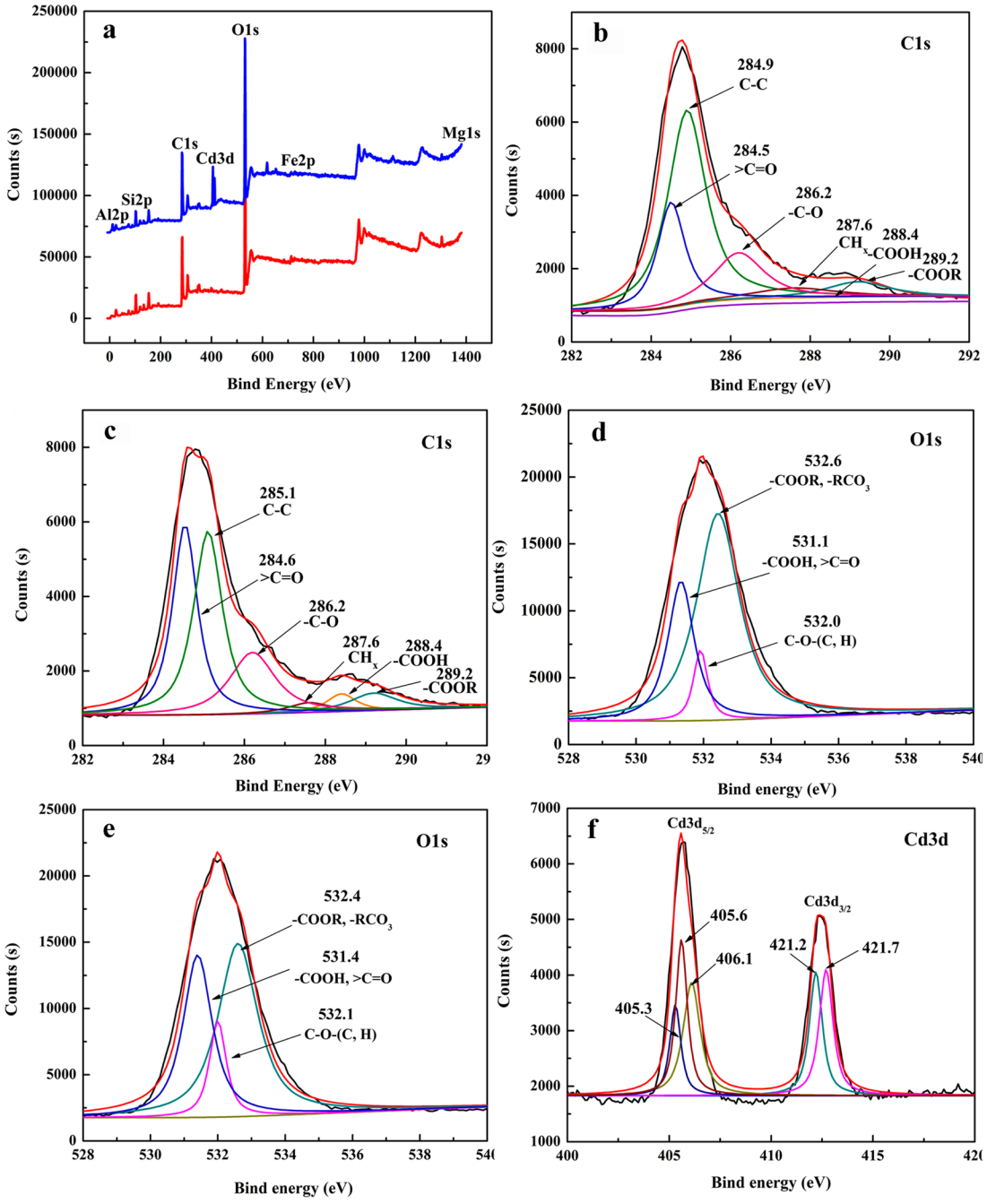

Figure 12. XPS spectra of wide scan, C 1s and O 1s for APT/C-300 before (a, b, d) and after (a, c, e) Cd(II) adsorption. Cd 3d spectra for APT/C-300 with Cd(II) uptake (f).

carboxylic groups, ketone, ester, phenol and ether could donate their electrons to the Cd(II) ions for the formation of coordination complexes or covalent binding.[60]

CONCLUSION

The APT/C naocomposites based on the SBE was prepared through one-step calcination used as the adsorbent to remove Cu(II), Pb(II) and Cd(II) from the single solutions. The as-prepared adsorbent exhibits a faster adsorption equilibrium and higher adsorption capacities for divalent heavy metal ions with the adsorption capacity of 32.32 mg/g for Cu(II), 46.72 mg/g for Cd(II) and 105.61 mg/g for Pb(II), respectively. The as-prepared nanocomposite displays an excellent desorption performance and reusable ability for heavy metal ions adsorption and after the fifth adsorption−desorption processes, making it a favorable material for facilitating the reuse of valuable metals, especially for Cu(II). Based on the results of the adsorption studies and XPS analysis for the APT/C nanocomposites before and after Cd(II) adsorption, the Cd(II) adsorption on the nanocomposites is mainly attributed to electrostatic attraction, ion exchange and surface complexation between the Cd(II) and the adsorbents. In summary, APT/C nanocomposites calcinated at 300 °C have promising potential for the removal of Cu(II), Pb(II) and Cd(II) from effluents applicable in industry, agriculture and other fields in large scale for their facile and green process, low toxicity and cost and high efficiency.

DOI: 10.1021/acssuschemeng.5b00040
ACS Sustainable Chem. Eng. 2015, 3, 1125−1135

AUTHOR INFORMATION

Corresponding Author

*A. Q. Wang. Tel.: +86 931 4968118. Fax: +86 931 8277088. E-mail: aqwang@licp.cas.cn.

Notes

The authors declare no competing financial interest.

ACKNOWLEDGMENTS

The authors thank "863" Project of the Ministry of Science and Technology, P. R. China (No. 2013AA032003) and the National Natural Science Foundation of China (No. 21377135) for the financial support of this research.

REFERENCES

(1) Celik, A.; Demirbas, A. Removal of heavy metal ions from aqueous solutions via adsorption onto modified lignin from pulping wastes. *Energy Sources* **2005**, *27*, 1167−1177.

(2) Garg, U. K.; Kaur, M. P.; Garg, V. K.; Sud, D. Removal of hexavalent Cr from aqueous solutions by agricultural waste biomass. *J. Hazard. Mater.* **2007**, *140*, 60−68.

(3) Zheng, Y. A.; Wang, A. Q. Removal of heavy metals using polyvinyl alcohol semi-IPN poly(acrylic acid)/tourmaline composite optimized with response surface methodology. *Chem. Eng. J.* **2010**, *162*, 186−193.

(4) Yan, L. L.; Kong, L.; Qu, Z.; Li, L.; Shen, G. Q. Magnetic biochar decorated with ZnS nanocrytals for Pb(II) removal. *ACS Sustainable Chem. Eng.* **2015**, *3*, 125−132.

(5) Asberry, H. B.; Kuo, C. Y.; Gung, C. H.; Conte, E. D.; Suen, S. Y. Characterization of water bamboo husk biosorbents and their application in heavy metal ion trapping. *Microchem. J.* **2014**, *113*, 59−63.

(6) Rao, R. A. K.; Ikram, S. Sorption studies of Cu(II) on gooseberry fruit (*Emblica officinalis*) and its removal from electroplating wastewater. *Desalination* **2011**, *277*, 390−398.

(7) He, J. S.; Chen, J. P. A comprehensive review on biosorption of heavy metals by algal biomass: Materials, performances, chemistry, and modeling simulation tools. *Bioresour. Technol.* **2014**, *160*, 67−78.

(8) Anna, W. K.; Roman, G. S.; Szymon, M. Biosorption of heavy metals from aqueous solutions onto peanut shell as a low-cost biosorbent. *Desalination* **2011**, *265*, 126−134.

(9) Liu, P.; Jiang, L. P.; Zhu, L. X.; Wang, A. Q. Novel approach for attapulgite/poly(acrylic acid) (ATP/PAA) nanocomposite microgels as selective adsorbent for Pb(II) ion. *React. Funct. Polym.* **2014**, *74*, 72−80.

(10) Liu, Y.; Kang, Y. R.; Mu, B.; Wang, A. Q. Attapulgite/bentonite interactions for methylene blue adsorption characteristics from aqueous solution. *Chem. Eng. J.* **2014**, *237*, 403−410.

(11) Wang, D. J.; Chen, H.; Xu, H.; Sun, J. M.; Xu, Y. Y. Preparation of wheat straw matrix-g-polyacrylonitrile-based adsorbent by SET-LRP and its applications for heavy metal ion removal. *ACS Sustainable Chem. Eng.* **2014**, *2*, 1843−1848.

(12) Sud, D.; Mahajan, G.; Kaur, M. P. Agricultural waste material as potential adsorbent for sequestering heavy metal ions from aqueous solutions - A review. *Bioresour. Technol.* **2008**, *99*, 6017−6027.

(13) Villela, A. A.; Jaccoud, D. B.; Rosa, L. P.; Freitas, M. V. Status and prospects of oil palm in the Brazilian Amazon. *Biomass Bioenergy* **2014**, *67*, 270−278.

(14) Vincent, C. J.; Shamsudin, R.; Baharuddin, A. S. Pre-treatment of oil palm fruits: A review. *J. Food Eng.* **2014**, *143*, 123−131.

(15) Foo, K. Y.; Hameed, B. H. Dynamic adsorption behavior of methylene blue onto oil palm shell granular activated carbon prepared by microwave heating. *Chem. Eng. J.* **2012**, *203*, 81−87.

(16) Husain, Z.; Zainal, Z. A.; Abdullah, M. Z. Analysis of biomass-residue-based cogeneration system in palm oil mills. *Biomass Bioenergy* **2003**, *24*, 117−124.

(17) Tan, I. A. W.; Ahmad, A. L.; Hameed, B. H. Fixed-bed adsorption performance of oil palm shell-based activated carbon for removal of 2,4,6-trichlorophenol. *Bioresour. Technol.* **2009**, *100*, 1494−1496.

(18) Foo, K. Y.; Hameed, B. H. Microwave-assisted preparation and adsorption performance of activated carbon from biodiesel industry solid reside: Influence of operational parameters. *Bioresour. Technol.* **2012**, *103*, 398−404.

(19) Zheng, Y. A.; Wang, A. Q. Granular hydrogel initiated by Fenton reagent and their performance on Cu(II) and Ni(II) removal. *Chem. Eng. J.* **2012**, *200*−*202*, 601−610.

(20) Du, H. Y.; Zhang, Z. Q.; Zhang, Y. N.; Li, M. Q. Study on colour reaction of xylenol orange with Pb(II) complex and its application. *J. Baoji Univ. Arts Sci., Nat. Sci. Ed.* **2009**, *29*, 35−40.

(21) Jiang, G. H.; Tang, Y. L.; Liu, L. Xylenol orange spectrophotometric determination of trace of Cd(II). *J. Changchun Normal Univ.* **1998**, *1*, 12−14.

(22) Zhou, J.; Liu, N.; Li, Y.; Ma, Y. J. Microscopic structure characteristics of attapulgite. *Bull. Chin. Ceram. Soc.* **1999**, *6*, 50−55.

(23) Liu, P.; Jiang, L. P.; Zhu, L. X.; Wang, A. Q. Attapulgite/poly(acrylic acid) nanocomposite (ATP/PAA) hydrogels with multi-functionalized attapulgite (org-ATP) nanorods as unique cross-linker: Preparation optimization and selective adsorption of Pb(II) ion. *ACS Sustainable Chem. Eng.* **2014**, *2*, 643−651.

(24) Kadi, S.; Lellou, S.; Marouf-Khelifa, K.; Schott, J.; Gener-Batonneau, I.; Khelifa, A. Preparation, characterisation and application of thermally treated Algerian halloysite. *Microporous Mesoporous Mater.* **2012**, *158*, 47−54.

(25) Kuang, W.; Facey, G. A.; Detellier, C. Dehydration and rehydration of palygorskite and the influence of water on the nanopores. *Clays Clay Miner.* **2004**, *52*, 635−642.

(26) Cheng, H.; Yang, J.; Frost, R. L. Thermogravimetric analysis-mass spectrometry (TG-MS) of selected Chinese palygorskites-implications for structural water. *Thermochim. Acta* **2011**, *512*, 202−207.

(27) Liang, X. F.; Xu, Y. M.; Tan, X.; Wang, L.; Sun, Y. B.; Lin, D. S.; Sun, Y.; Qin, X.; Wang, Q. Heavy metal adsorbents mercapto and amino functionalized palygorskite: Preparation and characterization. *Colloids Surf., A* **2013**, *426*, 98−105.

(28) Frost, R. L.; Ding, Z. Controlled rate thermal analysis and differential scanning calorimetry of sepiolites and palygorskites. *Thermochim. Acta* **2003**, *397*, 119−128.

(29) Eliche-Quesada, D.; Corpas-Iglesias, F. A. Utilisation of spent filtration earth or spent bleaching earth from the oil refinery industry in clay products. *Ceram. Interfaces* **2014**, *40*, 16677−16687.

(30) Wang, W. B.; Kang, Y. R.; Wang, A. Q. In situ fabrication of Ag nanoparticles/attapulgite nanocomposites: Green synthesis and catalytic application. *J. Nanopart. Res.* **2014**, *16*, 1−8.

(31) Mendelovici, E.; Portillo, D. C. Organic derivatives of attapulgite. I. Infrared spectroscopy and X-ray diffraction studies. *Clays Clay Miner.* **1976**, *24*, 177−182.

(32) Tian, G. Y.; Kang, Y. R.; Mu, B.; Wang, A. Q. Attapulgite modified with silane coupling agent for phosphorus adsorption and deep bleaching of refined palm oil. *Adsorpt. Sci. Technol.* **2014**, *32*, 37−48.

(33) Yin, H. B.; Kong, M. Simultaneous removal of ammonium and phosphate from eutrophic waters using natural calcium-rich attapulgite-based versatile adsorbent. *Desalination* **2014**, *351*, 128−137.

(34) Chang, W. S.; Park, C. M.; Kim, J. H.; Kim, Y. U.; Jeong, G.; Sohn, H. J. Quartz (SiO_2): A new energy storage anode material for Li-ion batteries. *Energy Environ. Sci.* **2012**, *5*, 6895−6899.

(35) Wang, W. J.; Chen, H.; Wang, A. Q. Adsorption characteristics of Cd(II) from aqueous solution onto activated palygorskite. *Sep. Purif. Technol.* **2007**, *55*, 157−164.

(36) Chen, H.; Zhao, J.; Zhong, A. G.; Jin, Y. X. Removal capacity and adsorption mechanism of heat-treated attapulgite clay for methylene blue. *Chem. Eng. J.* **2011**, *174*, 143−150.

(37) Wan, S. L.; Ma, Z. Z.; Xue, Y.; Ma, M. H.; Xu, S. Y.; Qian, L. P.; Zhang, Q. R. Sorption of lead(II), cadmium(II), and copper(II) ions

DOI: 10.1021/acssuschemeng.5b00040
ACS Sustainable Chem. Eng. 2015, 3, 1125−1135

from aqueous solutions using tea waste. *Ind. Eng. Chem. Res.* **2014**, *53*, 3629−3635.
(38) Meng, J.; Feng, X. L.; Dai, Z. M.; Liu, X. M.; Wu, J. J.; Xu, J. M. Adsorption characteristics of Cu(II) from aqueous solution onto biochar derived from swine manure. *Environ. Sci. Pollut. R.* **2014**, *21*, 7035−7046.
(39) Mohan, D.; Kumar, H.; Sarswat, A.; Alexandre-Franco, M.; Pittman, C. U., Jr. Cadmium and lead remediation using magnetic oak wood and oak bark fast pyrolysis bio-chars. *Chem. Eng. J.* **2014**, *236*, 513−528.
(40) Putra, W. P.; Kamari, A.; Yusoff, S. N. M.; Ishak, C. F.; Mohamed, A.; Hashim, N.; Isa, I. M. Biosorption of Cu(II), Pb(II) and Zn(II) ions from aqueous solutions using selected waste materials: Adsorption and characterisation studies. *J. Encapsulation Adsorpt. Sci.* **2014**, *4*, 25−35.
(41) Paulino, Á. G.; Cunha, A. J. D.; Alfaya, R. V. D. S.; Alfaya, A. A. D. S. Chemically modified natural cotton fiber: A low-cost biosorbent for the removal of the Cu(II), Zn(II), Cd(II), and Pb(II) from natural water. *Desalin. Water Treat.* **2014**, *52*, 4223−4233.
(42) Kamari, A.; Yusoff, S. N. M.; Abdullah, F.; Putra, W. P. Biosorptive removal of Cu(II), Ni(II) and Pb(II) ions from aqueous solutions using coconut dregs residue: Adsorption and characterisation studies. *J. Environ. Chem. Eng.* **2014**, *2*, 1912−1919.
(43) Chen, Y. D.; Huang, M. J.; Chen, W. Q.; Huang, B. Adsorption of Cu(II) from aqueous solution using activated carbon derived from mangosteen peel. *BioResources* **2012**, *7*, 4965−4975.
(44) Mohan, D.; Kumar, H.; Sarswat, A.; Alexandre-Franco, M.; Pittman, C. U., Jr. Cadmium and lead remediation using magnetic oak wood and oak bark fast pyrolysis bio-chars. *Chem. Eng. J.* **2014**, *236*, 513−528.
(45) Mohan, D.; Pittman, C. U., Jr.; Bricka, M.; Smith, F.; Yancey, B.; Mohammad, J.; Steele, P. H.; Alexandre-Francof, M. F.; Gómez-Serrano, V.; Gong, H. Sorption of arsenic, cadmium, and lead by chars produced from fast pyrolysis of wood and bark during bio-oil production. *J. Colloid Interface Sci.* **2007**, *310*, 57−73.
(46) Choi, J. W.; Chung, S. G.; Hong, S. W.; Kim, D. J.; Lee, S. H. Development of an environmentally friendly adsorbent for the removal of toxic heavy metals from aqueous solution. *Water Air Soil Pollut.* **2012**, *223*, 1837−1846.
(47) Han, Y. X.; Boateng, A. A.; Qi, P. X.; Lima, I. M.; Chang, J. M. Heavy metal and phenol adsorptive properties of biochars from pyrolyzed switchgrass and woody biomass in correlation with surface properties. *J. Environ. Manage.* **2013**, *118*, 196−204.
(48) Wang, X. S.; Miao, H. H.; He, W.; Shen, H. L. Competitive adsorption of Pb(II), Cu(II), and Cd(II) ions on wheat-residue derived black carbon. *J. Chem. Eng. Data* **2011**, *56*, 444−449.
(49) Yang, J.; Wu, J. X.; Lü, Q. F.; Lin, T. T. Facile preparation of lignosulfonate−graphene oxide−polyaniline ternary nanocomposite as an effective adsorbent for Pb(II) ions. *ACS Sustainable Chem. Eng.* **2014**, *2*, 1203−1211.
(50) Auta, M.; Hameed, B. H. Coalesced chitosan activated carbon composite for batch and fixed-bed adsorption of cationic and anionic dyes. *Colloids Surf., B* **2013**, *105*, 199−206.
(51) Zhou, Y. T.; Nie, H. L.; Branford-White, C.; He, Z. Y.; Zhu, L. M. Removal of Cu^{2+} from aqueous solution by chitosan-coated magnetic nanoparticles modified with α-ketoglutaric acid. *J. Colloid Interface Sci.* **2009**, *330*, 29−37.
(52) Wang, X. H.; Zheng, Y. A.; Wang, A. Q. Fast removal of copper ions from aqueous solutionby chitosan-g-poly(acrylic acid)/attapulgite composites. *J. Hazard. Mater.* **2009**, *168*, 970−977.
(53) Bradley, W. F. The structural scheme of attapulgite. *Am. Mineral.* **1940**, *25*, 405−410.
(54) Heymann, K.; Lehmann, J.; Solomon, D.; Schmidt, M. W.; Regier, T. C 1s K-edge near edge X-ray absorption fine structure (NEXAFS) spectroscopy for characterizing functional group chemistry of black carbon. *Org. Geochem.* **2011**, *42*, 1055−1064.
(55) He, H.; Qian, T. T.; Liu, W. J.; Jiang, H.; Yu, H. Q. Biological and chemical phosphorus solubilization from pyrolytical biochar in aqueous solution. *Chemosphere* **2014**, *113*, 175−181.
(56) Wu, X. P.; Gao, P.; Zhang, X. L.; Jin, G. P.; Xu, Y. Q.; Wu, Y. C. Synthesis of clay/carbon adsorbent through hydrothermal carbonization of cellulose on palygorskite. *Appl. Clay Sci.* **2014**, *95*, 60−66.
(57) López, G. P.; Castner, D. G.; Ratner, B. D. XPS O 1s binding energies for polymers containing hydroxyl, ether, ketone and ester groups. *Surf. Interface Anal.* **1991**, *17*, 267−272.
(58) Yang, G. X.; Jiang, H. Amino modification of biochar for enhanced adsorption of copper ions from synthetic wastewater. *Water Res.* **2014**, *48*, 396−405.
(59) Shi, L.; Zhang, G.; Wei, D.; Yan, T.; Xue, X. D.; Shi, S. S.; Wei, Q. Preparation and utilization of anaerobic granular sludge-based biochar for the adsorption of methylene blue from aqueous solutions. *J. Mol. Liq.* **2014**, *198*, 334−340.
(60) Liu, H.; Gao, Q.; Dai, P.; Zhang, J.; Zhang, C. L.; Bao, N. Preparation and characterization of activated carbon from lotus stalk with guanidine phosphate activation: Sorption of Cd(II). *J. Anal. Appl. Pyrolysis* **2013**, *102*, 7−15.
(61) Liang, X. F.; Han, J.; Xu, Y. M.; Sun, Y. B.; Wang, L.; Tan, X. In situ field-scale remediation of Cd polluted paddy soil using sepiolite and palygorskite. *Geoderma* **2014**, *235*, 9−18.

DOI: 10.1021/acssuschemeng.5b00040
ACS Sustainable Chem. Eng. 2015, 3, 1125−1135